$\mathcal{R}$esearch in
$\mathcal{A}$stronomy and
$\mathcal{A}$strophysics

Study of variable stars associated with maser sources: G025.65+1.05

Andrey M. Sobolev[1], Anastasia P. Bisyarina[1], Stanislav Yu. Gorda[1] and Andrey M. Tatarnikov[2]

[1] Astronomical Observatory of the Ural Federal University, Ekaterinburg 620000, Russia; *Andrej.Sobolev@urfu.ru*
[2] Sternberg Astronomical Institute of Moscow State University, Universitetsky Ave. 13, Moscow, 119899, Russia

Abstract We report variation of K-band infrared (IR) emission in the vicinity of the G025.65+1.05 water and methanol maser source. New observational data were obtained with the 2.5 m telescope at the Caucasian Mountain Observatory (CMO) of Moscow State University on 2017–09–21 during a strong water maser flare. We found that the IR source situated close to the maser position had decreased brightness in comparison to archive data. This source is associated with a massive young stellar object (MYSO) corresponding to the compact IR source IRAS 18316–0602 (RAFGL 7009S). A similar decrease in K-brightness of the IR source close to the maser position was observed in March 2011 when the water maser experienced a period of increased activity. The dips in MYSO brightness can be related to the maser flare phases. Maser flares that are concurrent with dips in the IR emission can be explained if the lower IR radiation field enables a more efficient sink for the pumping cycle by allowing IR photons to escape the maser region.

Key words: techniques: photometric — infrared: stars — masers

1 INTRODUCTION

Significant increases of the infrared (IR) flux in the vicinity of flaring methanol masers were recently reported for NGC 6334I-MM1 (Hunter et al. 2017), S255 (Stecklum et al. 2016; Zinchenko et al. 2017) and G107.298+5.639 (Stecklum et al. 2018). Noteworthily, in NGC 6334I, high activity of the water and methanol masers was contemporaneous (Hunter et al. 2017; MacLeod et al. 2018), but Very Large Array observations of the water masers (Brogan et al. 2018) showed that the majority of flaring water maser emission originated from the synchrotron source north along the jet driven by the source MM1 while the water maser emission toward the flaring IR source MM1 dropped. Meanwhile, the water and methanol maser flares in G107.298+5.639 were alternating (Szymczak et al. 2016). Further, no significant flares or dimming of emission were reported for the water maser in S255 during the strong methanol maser flares which took place in 2015 and 2016 (Fujisawa et al. 2015; Szymczak et al. 2018). This shows that association between flares in IR continuum and in maser lines of different molecules can have different natures.

In this paper, we consider near-IR variability in the vicinity of the water maser source G025.65+1.05 which recently experienced strong flares (Lekht et al. 2018; Volvach et al. 2017b,a; Ashimbaeva et al. 2017). The vicinity of this maser contains the compact IR source IRAS 18316–0602 (RAFGL 7009S) with luminosity of about $3 \times 10^4 \, L_\odot$ (McCutcheon et al. 1995) and the ultracompact HII region G025.65+1.05. The radio source, first identified at 3.6 cm by Kurtz et al. (1994), coincides spatially with submillimeter emission at 350 μm (Hunter et al. 2000), 450 and 850 μm (Walsh et al. 2003). The region contains a massive young stellar object (YSO) which drives CO bipolar outflow (Shepherd & Churchwell 1996). Zavagno et al. (2002) suggest that RAFGL 7009S is an embedded YSO "associated with the ultracompact HII region G025.65+1.05, which may be excited by a B1V star". Kinematic distance estimation based on ammonia line observations gives the value of about 3.2 kpc (e.g. Molinari et al. 1996).

A prominent bright rapid flare in the main feature of the water maser took place in September 2017 – flux density increased from less than 1 kJy to about 20 kJy in a few days (Volvach et al. 2017b). This flare and the previous one were preceded by a moderate rise in the methanol maser

emission which happened 3 months in advance of the water maser flare (Sugiyama et al. 2017). There were two more bright flares in October-November (Volvach et al. 2017a; Ashimbaeva et al. 2017). The latter one lasted only for a couple of days, reached 76 kJy at the maximum and faded to 16 kJy within a day (Ashimbaeva et al. 2017).

We obtained K-band data of G025.65+1.05 on 2017–09–21 (soon after the peak of the first maser flare) at the Caucasian Mountain Observatory (CMO), administered by the Sternberg Astronomical Institute of Moscow State University. Variation of G025.65+1.05 K-band flux density distribution was noticed "by eye" after comparison with an archive UKIDSS image (Sobolev et al. 2017). First photometric data were given in Stecklum et al. (2017). In this paper, we present a new photometric study of G025.65+1.05 IR-variability.

2 CMO OBSERVATIONS

Observations of G025.65+1.05 were obtained at CMO on 2017–09–21 in the IR K-band using ASTRONIRCAM (Nadjip et al. 2017). The instrumental photometric system is close to the standard Mauna Kea Observatory (MKO) photometric system. The camera was set in imaging mode. The final image is the sum of 50 separate images obtained with an exposure of 3.67 seconds with $3''$ dithering. For these separate images, the bias, dark and flat-field correction were applied. The FWHM (CMO point-spread function) of the resulting image is about $1.1''$.

On the date of the CMO observations, the flux density of the water maser was about 15 kJy (Volvach A. E., private communication). We also used archival IR data and data from previous observations in the literature. Data and references are listed in Table 1.

3 DATA REDUCTION

We analyzed the flux density distribution along a chosen line passing through the considered source. The flux density was integrated in the tangential direction within the width of a rectangle with the size of $75'' \times 6''$ (shown in Fig. 1). It contains three IR sources close to the maser position and three isolated stars used for calibration and calibration control. The width of the rectangle was chosen in order to cover at least 90 per cent of emission from these objects. We calibrated the data to uniform scale assuming that the star marked 4 does not vary. Photometric analysis had shown that this star varied only within the limits of 0.1 mag from its mean value for all our data. Extreme variations of this star were the following: magnitude of

star 4 increased by about 0.1 mag on 2007–08–27 and decreased on 2011–09–17 by about the same value. Images from these dates were obtained by UKIDSS. So, we used the average signal to get the UKIDSS data calibration parameters.

The numerical scale of obtained flux density was derived from the 2MASS K-flux for star 4. The calibration coefficients were found by fitting the integrated observed signal of star 4 and it absolute flux density, calculated from the 2MASS point source catalog value $K = 14.525$ mag. To facilitate comparison of the data, we smoothed images in order to have the same angular resolution as in CMO observations (convolution process). The convolution was conducted with the IRAF software. The resulting flux density profiles are shown in Figures 2 and 3. We did not attempt to obtain exact absolute values of the flux densities because further considerations are based on analysis of the relative flux density changes.

4 RESULTS AND DISCUSSION

Figures 2 and 3 indicate that the IR source nearest to the maser position (marked by 1 in the figures) was significantly fainter in September 2017 and March 2011 in comparison to other epochs. Note that the image from March 2011 was obtained with OSIRIS/SOAR using a narrow continuum filter centered at 2.14 μm (C2 in Table 1) while the other images were obtained with broad K-band filters. In September 2011 the emission of the source was slightly dimmer compared to the majority of the epochs. We think that the low flux density in the SOAR data is likely due to actual variability and not to calibration artifacts.

The epoch of our CMO observation is close to the maser flare. Consideration of the results of long-term water maser monitoring by Lekht et al. (2018) shows that the epochs of IR observations in 2011 correspond to the periods of increased maser activity (with several kJy in March and about 400 Jy in September). The other epochs presented in Table 1 correspond to a considerably lower state of maser activity with flux densities less than 200 Jy. Therefore, our analysis points to a possible connection between water maser flares and dips in IR emission.

A half a day rise and two day duration of the recent maser flare reported by Ashimbaeva et al. (2017) imply that the flare is caused by changes in the radiative part of the pumping process since the geometrical changes and collisional events are expected to be slower: even in W49N with its extremely powerful (for such interstellar objects) shocks, the time duration of the fastest detected flare is considerably longer (Liljeström & Gwinn 2000).

Table 1 Observational Data

| Date (YYYY–MM–DD)	MJD	Instrument	Filter	λ_{central} (μm)	$\Delta\lambda$ (μm)
2003–06–16	52806.4	UFTI, UKIRT	K	2.20	0.34
2004–07–11	53197.7	IRIS2, AAT	K_s	2.14	0.32
2007–08–27	54339.3	WFCAM, UKIRT	K	2.20	0.34
2011–03–20	55640.4	OSIRIS, SOAR	C2	2.14	0.05
2011–09–18	55822.3	WFCAM, UKIRT	K	2.20	0.34
2017–09–21	58017.6	CMO	K	2.19	0.32

Notes: UFTI data are reported in Varricatt et al. (2010), AAT data in Longmore et al. (2006) and SOAR data in Navarete et al. (2015).
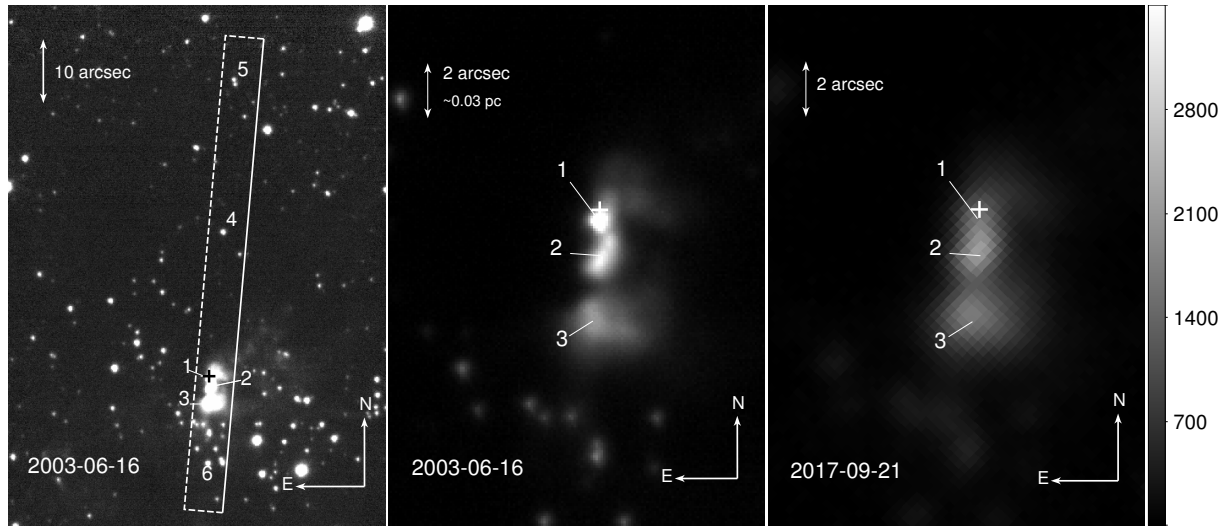
Fig. 1 Vicinity of G025.65+1.05 in K-band. The water maser position from Jenness et al. (1995) is marked by a *cross*. The *rectangle* in the left panel shows the region in which flux density distribution is measured. Numbers 1 and 2 indicate the peak positions of the IR sources nearest to the water maser position. Star 4 was used for calibration, and stars 5 and 6 for calibration control. The two left panels display data obtained on 2003–06–16 in different spatial and brightness scales. The spatial scale is given at the top of each panel, and the distance from the source is taken from Molinari et al. (1996). The right panel shows the CMO data with the same brightness scale as the central image. The numerical scale in units 10^{-18} W m^{-2} μm^{-1} arcsec^{-2} is based on a 2MASS catalog value for star 4. The marked positions of sources 1–3 in the right panel are taken from peak positions of the central image. The flux density decrease of source 1 in 2017 is clearly seen.

Substantial influence of the radiative processes is very likely because they play a very important role in the water maser pumping (Gray 2012; Gray et al. 2016). Since water maser flares presumably happen during dips in the IR emission, it is not likely that the IR radiation makes the main contribution to the source of the maser pumping. This corresponds to results of theoretical considerations which show that pumping of the strong water masers with the radiative source is unlikely (Strelnitskii 1984; Deguchi 1981; Shmeld 1976) because the pump power in these cases is insufficient. We have to note that an analysis of the role of IR radiation in the pumping without consideration of the maser sink is not complete. The sink for the pumping is often ignored but it can play a crucial role in maser formation (Strelnitskii 1981; Sobolev & Gray 2012). For water masers, theoretical considerations show that the sink for the IR photons due to cold dust absorption within the masing region can produce strong masers (for a far IR photon sink (Deguchi 1981) and for a near IR photon sink (Strelnitskii 1977)). The alternating character of IR radiation density and water maser activity finds observational support in the drop of water maser flux accompanied by the increase in the radiation field, as was recently observed in NGC 6334I-MM1 by Brogan et al. (2018).
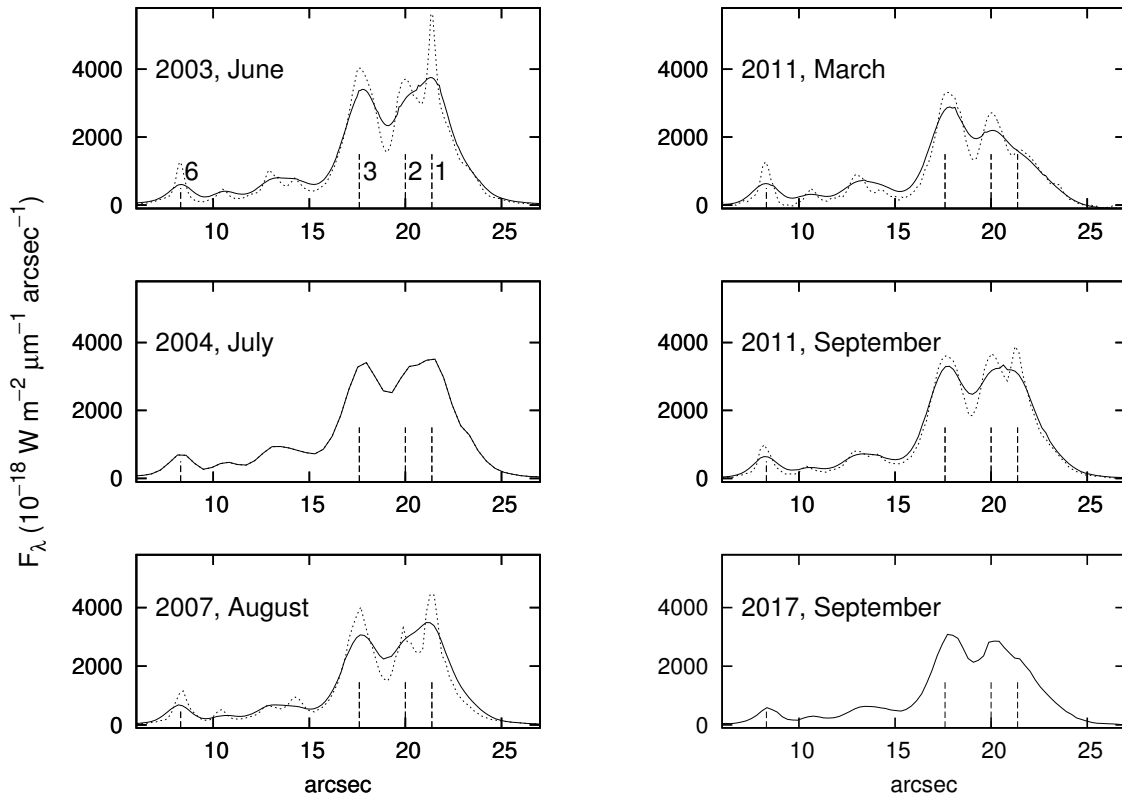
Fig. 2 The flux density distribution along the *rectangle* shown in Fig. 1. The vertical scale is rough and was obtained from the $K = 14.525$ mag 2MASS catalog value for star 4. The horizontal scale represents the angular distance (in arcsecond) from (J2000): RA $= 18^\mathrm{h}34^\mathrm{m}20.952^\mathrm{s}$ and Dec $= -5°59'25.375''$. The *solid line* represents data after smoothing to the CMO angular resolution, and *dotted line* corresponds to data without angular smoothing (for cases when the angular resolution of the data is different from the CMO data one). The *dashed bar* marked by 1 indicates peak position of the IR source nearest to the water maser. The positions of sources, marked by *dashed bars* in all panels, are taken from the peak positions of the first panel image (2003–06–16, data with better angular resolution). The source designations are the same as in Fig. 1. The K-band intensity of source 1 was significantly less in March 2011 and September 2017 with respect to other epochs.

An increase of the water maser sink efficiency is also realized in the case when it is possible for IR photons to escape from the masing region. This possibility is blocked when radiation density in the surroundings of the masing region is high. Maser flares that are simultaneous with dips in the IR emission can be explained by the following effect: decrease in the IR radiation field increases efficiency of the sink for the pumping mechanism by allowing more IR photons to escape from the masing region.

At present, we do not have data describing changes in the near and far IR radiation density during the G025.65+1.05 maser flare, which are necessary for a full analysis of the situation. Anyhow, the low level of K-band intensity from the source during the flare can indicate that the density of radiation in the masing region is probably reduced at longer IR wavelengths as well. Such a situation takes place in the intermediate mass YSO G107.298+5.639. Recent observations of this source by

Stecklum et al. (2018) have shown that the periods of high water maser activity coincide with periods when the near-IR K-band and mid-IR NEOWISE W1, W2, W3 and W4 intensities of the source are reduced.

5 CONCLUSIONS

We report a variability study of IR K-band flux density in the G025.65+1.05 vicinity. The IR source nearest to the water maser had significantly lower IR flux densities in March 2011 and September 2017 with respect to other considered epochs of observations. These two epochs are close to epochs when the water maser was flaring. So, the epochs of the water maser flares can be related to the periods of K-band dips. We suggest that this relation is explained by the alternating character of the water maser sink efficiency and the IR radiation field density in the vicinity of the maser source.
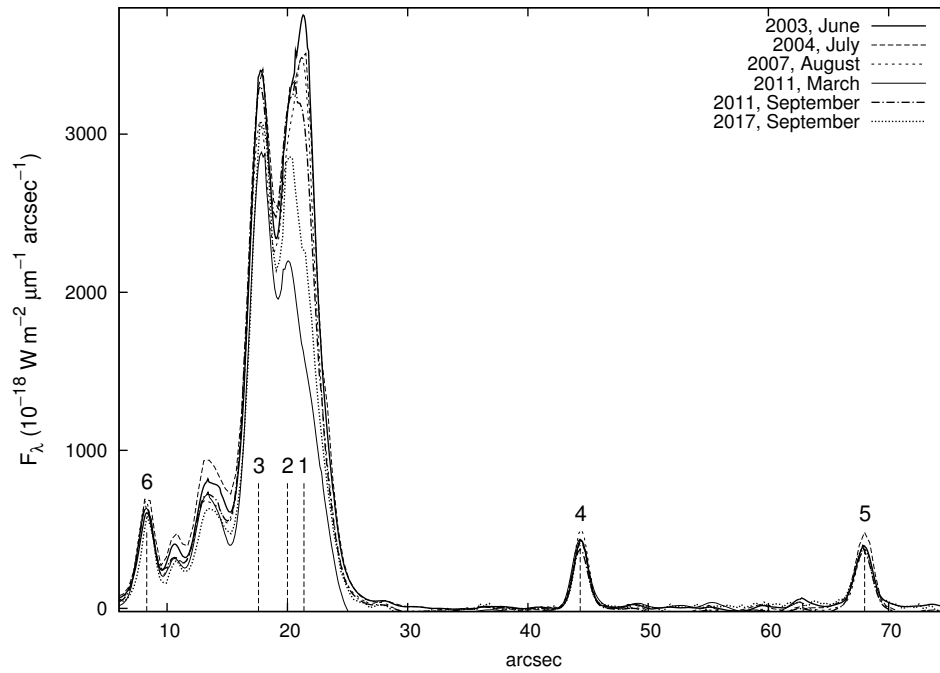
Fig. 3 Superposition of the flux density profiles along the *rectangle* shown in Fig. 1. The designations are similar to those in Fig. 1 and Fig. 2. Star 4 was used for calibration and stars 5 and 6 for calibration control. All data are smoothed to the angular resolution of CMO. Source 1 was significantly fainter in March 2011 and September 2017 with respect to the other epochs.

References

Ashimbaeva, N. T., Platonov, M. A., Rudnitskij, G. M., & Tolmachev, A. M. 2017, The Astronomer's Telegram, 11042

Brogan, C. L., Hunter, T. R., Cyganowski, C. J., et al. 2018, ApJ, 866, ,87

Deguchi, S. 1981, ApJ, 249, 145

Fujisawa, K., Yonekura, Y., Sugiyama, K., et al. 2015, The Astronomer's Telegram, 8286

Gray, M. 2012, Maser Sources in Astrophysics (Cambridge, UK: Cambridge University Press)

Gray, M. D., Baudry, A., Richards, A. M. S., et al. 2016, MNRAS, 456, 374

Hunter, T. R., Churchwell, E., Watson, C., et al. 2000, AJ, 119, 2711

Hunter, T. R., Brogan, C. L., MacLeod, G., et al. 2017, ApJ, 837, L29

Jenness, T., Scott, P. F., & Padman, R. 1995, MNRAS, 276, 1024

Kurtz, S., Churchwell, E., & Wood, D. O. S. 1994, ApJS, 91, 659

Lekht, E. E., Pashchenko, M. I., Rudnitskii, G. M., & Tolmachev, A. M. 2018, Astronomy Reports, 62, 213

Liljeström, T., & Gwinn, C. R. 2000, ApJ, 534, 781

Longmore, S. N., Burton, M. G., Minier, V., & Walsh, A. J. 2006, MNRAS, 369, 1196

MacLeod, G. C., Smits, D. P., Goedhart, S., et al. 2018, MNRAS, 478, 1077

McCutcheon, W. H., Sato, T., Purton, C. R., Matthews, H. E., & Dewdney, P. E. 1995, AJ, 110, 1762

Molinari, S., Brand, J., Cesaroni, R., & Palla, F. 1996, A&A, 308, 573

Nadjip, A. E., Tatarnikov, A. M., Toomey, D. W., et al. 2017, Astrophysical Bulletin, 72, 349

Navarete, F., Damineli, A., Barbosa, C. L., & Blum, R. D. 2015, MNRAS, 450, 4364

Shepherd, D. S., & Churchwell, E. 1996, ApJ, 457, 267

Shmeld, I. K. 1976, Soviet Ast., 20, 571

Sobolev, A. M., Bisyarina, A. P., Tatarnikov, A. M., Antokhin, I., & Volvach, A. E. 2017, The Astronomer's Telegram, 10788, 1

Sobolev, A. M., & Gray, M. D. 2012, in IAU Symposium, 287, Cosmic Masers - from OH to H0, eds. R. S. Booth, W. H. T. Vlemmings, & E. M. L. Humphreys, 13

Stecklum, B., Caratti o Garatti, A., Cardenas, M. C., et al. 2016, The Astronomer's Telegram, 8732

Stecklum, B., Caratti o Garatti, A., Klose, S., & Wiseman, P. 2017, The Astronomer's Telegram, 10842

Stecklum, B., Caratti o Garatti, A., Hodapp, K., et al. 2018, in IAU Symposium, 336, Astrophysical Masers: Unlocking the Mysteries of the Universe, eds. A. Tarchi, M. J. Reid, & P. Castangia, 37

Strelnitskii, V. S. 1977, Soviet Ast., 21, 381

Strelnitskii, V. S. 1981, Soviet Ast., 25, 373

Strelnitskii, V. S. 1984, MNRAS, 207, 339

Sugiyama, K., Saito, Y., Akitaya, H., Yonekura, Y., & Momose, M. 2017, The Astronomer's Telegram, 10757

Szymczak, M., Olech, M., Wolak, P., Bartkiewicz, A., & Gawroński, M. 2016, MNRAS, 459, L56

Szymczak, M., Olech, M., Wolak, P., Gérard, E., & Bartkiewicz, A. 2018, A&A, 617, A80

Varricatt, W. P., Davis, C. J., Ramsay, S., & Todd, S. P. 2010, MNRAS, 404, 661

Volvach, A. E., Volvach, L. N., MacLeod, G., et al. 2017a, The Astronomer's Telegram, 10853

Volvach, A. E., Volvach, L. N., MacLeod, G., et al. 2017b, The Astronomer's Telegram, 10728

Walsh, A. J., Macdonald, G. H., Alvey, N. D. S., Burton, M. G., & Lee, J.-K. 2003, A&A, 410, 597

Zavagno, A., Deharveng, L., Nadeau, D., & Caplan, J. 2002, A&A, 394, 225

Zinchenko, I., Liu, S.-Y., Su, Y.-N., & Sobolev, A. M. 2017, A&A, 606, L6